

High-sensitivity refractive index sensors based on Fano resonance in a metal-insulator-metal based arc-shaped resonator coupled with a rectangular stub

Shubin Yan(闫树斌), Hao Su(苏浩), Xiaoyu Zhang(张晓宇), Yi Zhang(张怡), Zhanbo Chen(陈展博), Xiushan Wu(吴秀山), and Ertian Hua(华尔天)

Citation: Chin. Phys. B, 2022, 31 (**10**): 108103. DOI: 10.1088/1674-1056/ac76ac
Journal homepage: http://cpb.iphy.ac.cn; http://iopscience.iop.org/cpb

What follows is a list of articles you may be interested in

Optical strong coupling in hybrid metal-graphene metamaterial for terahertz sensing

Ling Xu(徐玲), Yun Shen(沈云), Liangliang Gu(顾亮亮), Yin Li(李寅), Xiaohua Deng(邓晓华), Zhifu Wei(魏之傅), Jianwei Xu(徐建伟), and Juncheng Cao(曹俊诚)

Chin. Phys. B, 2021, 30 (**11**): 118702. DOI: 10.1088/1674-1056/abfb58

Terahertz multi-metal-wire hybrid-cladding hollow waveguide for refractive index sensing

Ying-Ying Yu(于莹莹), Xu-You Li(李绪友), Kun-Peng He(何昆鹏), Bo Sun(孙波)

Chin. Phys. B, 2016, 25 (**2**): 028703. DOI: 10.1088/1674-1056/25/2/028703

High-sensitivity refractive index sensors based on Fano resonance in a metal-insulator-metal based arc-shaped resonator coupled with a rectangular stub

Shubin Yan(闫树斌)[1,†], Hao Su(苏浩)[2], Xiaoyu Zhang(张晓宇)[3], Yi Zhang(张怡)[1], Zhanbo Chen(陈展博)[1], Xiushan Wu(吴秀山)[1], and Ertian Hua(华尔天)[1]

[1] *School of Electrical Engineering, Zhejiang University of Water Resources and Electric Power, Zhejiang–Belarus Joint Laboratory of Intelligent Equipment and System for Water Conservancy and Hydropower Safety Monitoring, Hangzhou* 310018, *China*

[2] *Hangzhou Hikvision Digital Technology Co., Ltd., Hangzhou* 310018, *China*

[3] *School of Electrical and Control Engineering, North University of China, Taiyuan* 030051, *China*

(Received 18 April 2022; revised manuscript received 27 May 2022; accepted manuscript online 8 June 2022)

A metal-insulator-metal (MIM)-based arc-shaped resonator coupled with a rectangular stub (MARS) structure is proposed. This structure can generate two tunable Fano resonances originating from two different mechanisms. The structure has the advantage of being sensitive to the refractive index, and this feature makes it favorable for application in various microsensors. The relationship between the structural parameters and Fano resonance is researched using the finite element method (FEM) based on the software COMSOL Multiphysics 5.4. The simulation reveals that the sensitivity reaches 1900 nm/refractive index unit (RIU), and the figure of merit (FOM) is 23.75.

Keywords: Fano resonance, metal-insulator-metal (MIM) waveguide, refractive index sensor, Fabry–Perot (F-P) cavity

PACS: 81.07.Oj, 87.85.Ox **DOI:** 10.1088/1674-1056/ac76ac

1. Introduction

Surface plasmon polaritons (SPPs) can break through the diffraction limit and confine light in the sub-wavelength range.[1] When incident photons are coupled to the electrons on the conductor's surface, SPPs will occur. Research on SPP-based metal-insulator-metal (MIM) waveguides has attracted the attention of researchers worldwide. In recent years, the SPP-based MIM waveguide has been applied in many areas, such as filters,[2–5] sensors,[6–9] and slow light systems.[10] These applications promote the rapid development of novel instruments.

The Fano resonance effect emerges from the coupling and interference of a non-radiative or continuum of the radiative spectrum.[11–13] Fano resonance exhibits an asymmetrical and ultra-sharp shape compared to the Lorentzian-shaped resonance. Because of its ultra-sharp transmission spectrum, Fano resonance has been applied in sensing equipment.[14,15] By detecting the small changes in ambient parameters, equipment based on Fano resonance can monitor changes in refractive index. In recent years, the design based on the structure of the MIM waveguide has been widespread. Qian Yang proposed a MIM waveguide structure comprised of a cross-shaped resonator, and the value of its sensitivity is 1075 nm/refractive index unit (RIU).[16] The Fano resonance of the structure can be tunable by changing the resonator's length parameters. Jialing He designed a structure consisting of a ring resonator and a stub coupled with a MIM waveguide. The structure's sensitivity is 1100 nm/RIU, and the figure of merit (FOM) reaches 42550.[17] Cheng Zhang proposed a simple waveguide-microring Fano structure and applied it to temperature measurement.[18]

This study proposes a MIM-based arc-shaped resonator coupled with a rectangular stub (MARS) structure. This structure can generate two tunable Fano resonances, including Fano resonance 1 (FR1) and Fano resonance 2 (FR2). The wavelength of FR1 is between 1400 nm and 2000 nm, and FR2 is between 800 nm and 1200 nm). To understand the formation principles of Fano resonances, this study adds three other structures to conduct comparative experiments. The size of the structure is controlled by hundreds of nanometers. The structure is sensitive to the changes in the surrounding environmental parameters and has the potential to be applied to various microsensors. The relationship between the structural parameters and Fano resonance is researched using the finite element method (FEM) based on the software CMOSOL Multiphysics 5.4. The simulation reveals that the sensitivity can reach 1900 nm/RIU and the FOM is 23.75. Refractive index sensors based on Fano resonance have proven to be efficient. However, due to the limits of etching precision, it is difficult to precisely take control of the distance d and manufacture the MARS resonance cavity system.[19,20] This study mainly analyzes the formation principles and influencing factors theoretically and provides experience for manufacturing in the future.

[†]Corresponding author. E-mail: yanshb@zjweu.edu.cn

© 2022 Chinese Physical Society and IOP Publishing Ltd

2. Structure model and analysis method

A 2D illustrative diagram of the MARS structure proposed in this study, composed of a MIM with a rectangular stub coupled with the arc-shaped resonant cavity, is shown in Fig. 1. The white part represents the dielectric layer of air, and the green part indicates metal Ag separately. R_1 and R_2 are the radii of the inner and outer arc-shaped resonator, respectively; r_1, r_2 and r_3 are the radii of the three inner circles, respectively; d is used to describe the distance between the arc-shaped resonant cavity and MIM waveguide, and h indicates the height of the rectangular stub.

We choose the air as the isolators in the MIM waveguide and the arc-shaped resonator ($n_\mathrm{d} = 1$). The Ag is chosen to be the metal-dielectric, whose relative dielectric constant (ε_d) can be described by[21]

$$\varepsilon_\mathrm{d}(\omega) = \varepsilon_\infty - \frac{\omega_\mathrm{p}^2}{\omega(\omega + \mathrm{i}\gamma)}. \tag{1}$$

Herein, ω represents the angular frequency of an incident wave in a vacuum, the infinite dielectric constant ε_∞ is 3.7, the angular frequency of the plasma oscillation ω_p is equal to 9.1 eV (1.38×10^{16} rad/s), and the frequency of electron collision γ is 0.018 eV (2.73×10^{13} rad/s).

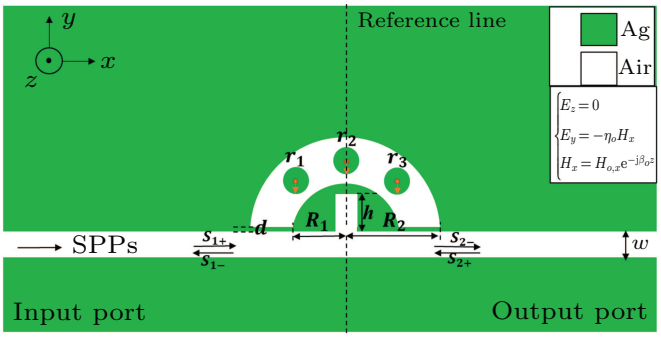


Fig. 1. A 2D schematic of the structure comprising a MIM with a rectangular stub coupled with the arc-shaped resonant cavity.

To ensure that only the fundamental transverse magnetic (TM) exists in the MIM waveguide, w is set to 50 nm. The TM is characterized by the field amplitude decaying exponentially into both media away from the interface.[22] The electric field intensity of the z-axis and y-axis, and the magnetic field intensity of the x-axis are shown on the right-hand side of Fig. 1. The top and bottom boundaries are the perfectly matched layers (PMLs). With the help of FEM,[23] the transmission spectrum of the structure can be obtained. The trajectory of incident light is from the input port P_1 to the output port P_2. Here, S_{1+}, S_{1-}, S_{2+} and S_{2-} are the scattering parameters of the incident light.

3. Simulation and results

To understand the formation principles of Fano resonances, this study adds three other structures, including a structure without the rectangular stub, a structure without three circles in the arc-shaped resonant cavity, and a structure without the arc-shaped resonant cavity. By comparing the different transmission spectrums of four structures, it is easy to learn about the formation process of Fano resonance. The transmission spectra of these four structures are shown in Fig. 2.

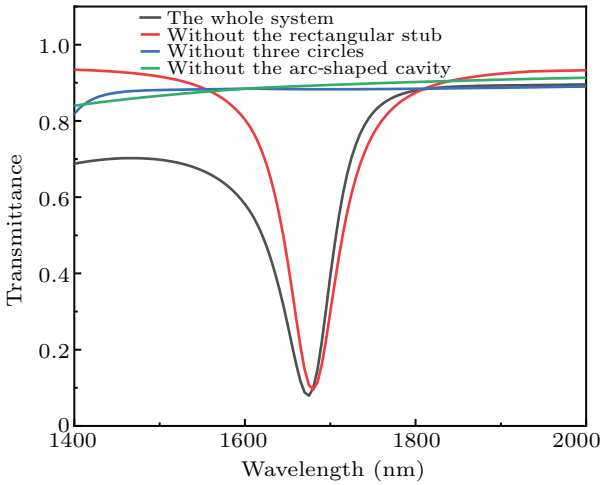


Fig. 2. The transmission spectrum of the whole system (the black line), without the rectangular stub (the red line), without three circles in the arc-shaped resonant cavity (the blue line), and without the arc-shaped cavity (the green line).

From the principle of resonance formation, Fano resonance will be generated when the continuous wide-band state interacts with the discrete narrow-band state. It is the MIM waveguide that provides the continuous broad-band-state mode. It can be seen that when adding the arc-shaped resonant cavity, the FR1 occurs at the wavelength of 1673.5 nm. The arc-shaped resonator generates the discrete narrow-band state mode in the formation of Fano resonance. In addition, by comparing the red curve with the black curve, it is easy to find that the FR2 is formed at the wavelength of 1070 nm when the rectangular stub is added. The rectangular stub can be approximately regarded as a Fabry–Perot (F-P) cavity. The air medium layer is sandwiched between two silver medium layers, which form a grating structure. This structure makes the directly transmitted light and the diffracted light interfere easily. It can be seen in Fig. 3(a) that when the rectangular stub is added to the structure, stronger resonance occurs in the arc-shaped resonant cavity and, at this time, SPPs are practically limited in the arc-shaped one.

When the three circles do not exist in the arc-shaped resonant cavity, two Fano resonances also form at 1030 nm and 1295 nm. The arc-shaped resonant cavity and the rectangular stub make two Fano resonances. In contrast, the circles inside the cavity make the dip of the Fano resonances move towards longer wavelengths and increase the wavelength differences between two Fano resonances. Meantime, the full width at the half maximum (FWHM) also becomes smaller, which is the

reason for the more significant FOM value, and it is our goal to obtain the significant FOM value.

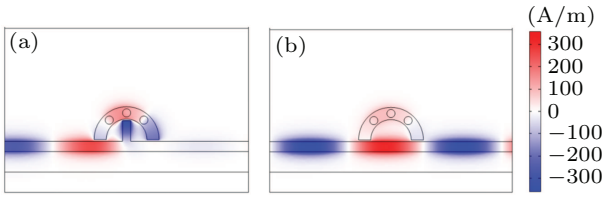


Fig. 3. The distribution of the Hz field in the dip of 1070 nm: (a) with and (b) without the rectangular stub.

To evaluate the sensing performance of the Fano system, two vital indices, including sensitivity and FOM, are introduced to the following experiments. The formulas of the sensitivity and FOM can be expressed by

$$S = \frac{\Delta\lambda}{\Delta n}, \tag{2}$$

$$\mathrm{FOM} = \frac{S}{\mathrm{FWHM}}. \tag{3}$$

Herein, $\Delta\lambda$ and Δn are the changes in the wavelength and refractive indices, respectively.

Figure 4(a) shows that when the refractive index changes from 1.00 to 1.05 at an interval of 0.01, the transmission spectrum shows a redshift. According to Eq. (2), when $d = 8$ nm, $h = 100$ nm, $R_1 = 176$ nm, $R_2 = 110$ nm, and $r_1 = r_2 = r_3 = 22$ nm, the sensitivity reaches 1900 nm/RIU, which makes it efficient to detect changes in the refractive index.

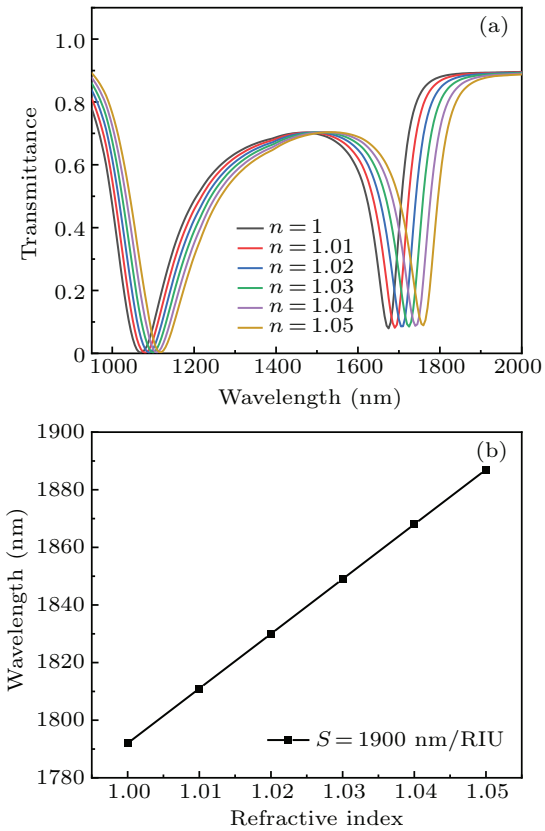


Fig. 4. (a) The transmission spectrum shows a redshift when changing the refractive indices; (b) the sensitivity curve of Fano resonance.

The proposed structure can be used to detect the changes in the refractive index. Assuming the initial refractive index is 1.00, the value increases from 1.00 to 1.05 at an interval of 0.01. The simulated transmission spectrum is shown in Fig. 4(a), from which it is evident that the dip of the Fano resonance moves to a longer wavelength. The parameter S can be used to reflect the performance of the structure. The structure designed in the article has a sensitivity of 1900 nm/RIU, which means the dip in the wavelength moves at a step of 19 nm. Therefore, we can calculate the refractive index according to the value of the resonance dip.

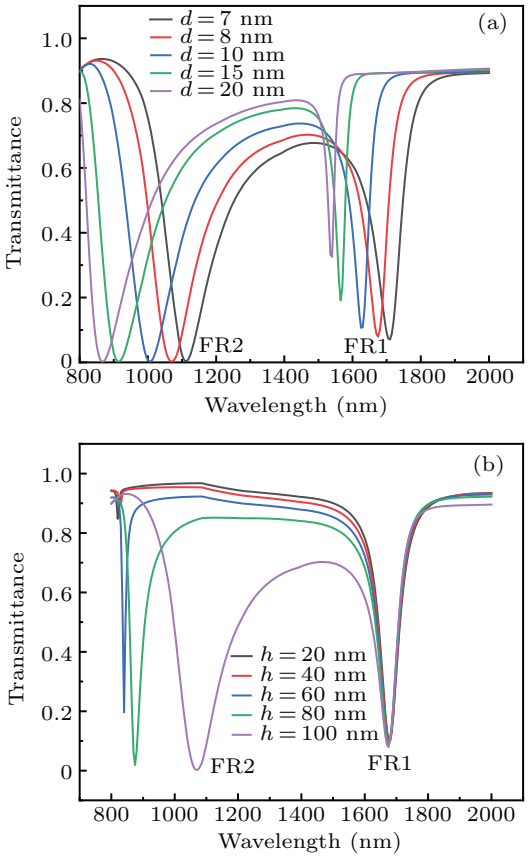


Fig. 5. The transmission spectrum of (a) different coupling distances between the arc-shaped resonant cavity and MIM waveguide d; (b) different heights of the rectangular stub h.

Next, the effects of changing several parameters such as d, h, R, and r are researched. Due to the more significant sensitivity value of FR1, FR1 is a primary study focus to help understand the effects of different parameters on the structure's sensitivity. As shown in Fig. 5(a), when d increases from 7 nm to 20 nm, the dip of FR1 increases sharply, while both FR1 and FR2 show a blueshift. The parameter d has a vital influence on the transmittance of FR1. In this study, d is chosen to be 8 nm. When $d = 7$ nm or smaller, the sensitivity curve linearity of the system is not good, limiting its application in sensors. Therefore, taking linearity and sensitivity into account, d is chosen to be 7 nm. As shown in Fig. 5(b), when h increases from 20 nm to 100 nm at an interval of 20 nm, the dip of FR1 is almost unchanged, while the dip of FR2 decreases

sharply. The height of the rectangular stub mainly exerts its influence on FR2. According to the simulation results, the sensitivity reaches 1900 nm/RIU when h is 100 nm. Considering the structural design, h should not be greater than 100 nm. Finally, h is chosen to be 100 nm.

In the resonator system of the MIM waveguide, the resonance wavelength of the peak can be calculated based on the standing wave theory as[24]

$$\lambda_m = \frac{2\mathrm{Re}(n_{\mathrm{eff}})L}{m-(\psi_{\mathrm{r}}/\pi)}, \tag{4}$$

where L is the length of the cavity, m is the antinodes number of the SPP wave, ψ_{r} describes the phase difference of the reflected beam, and $\mathrm{Re}(n_{\mathrm{eff}})$ represents the real part of the refractive index of a MIM waveguide.

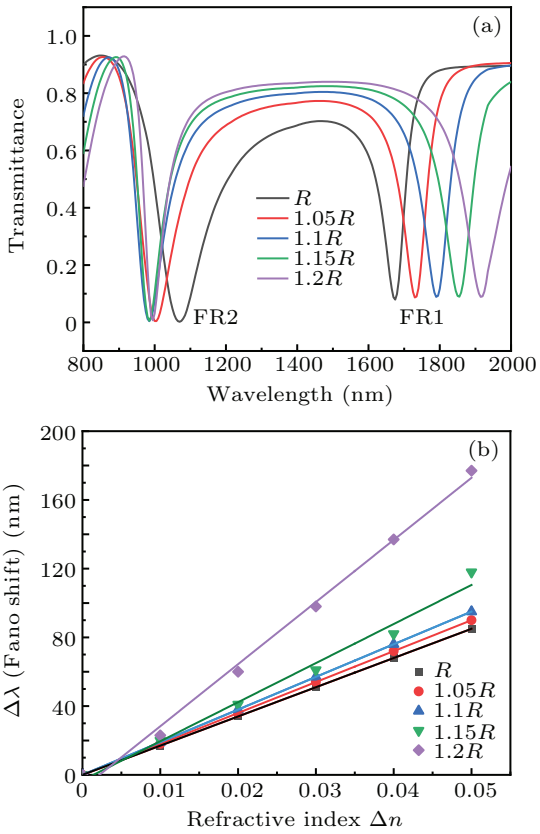


Fig. 6. (a) The transmission spectrum of different R; (b) the sensitivity curve of Fano resonance when R changes from R to 1.2R.

In the following part, we set the parameter R as a constant, and R represents the initial values of R_1, R_2, r_1, r_2, and r_3. The initial values of R_1 and R_2 are set to 160 nm and 100 nm, respectively. The r_1, r_2, and r_3 initial assignments are all 20 nm. When R_1, R_2, r_1, r_2, and r_3 vary from R to 1.2R, the dip of FR1 is redshifted, while the dip of FR2 moves to shorter wavelengths. As mentioned earlier, the generation of FR1 is relevant to the arc-shaped resonant cavity. When the radius increases to 1.2R, equal to the more significant value of the length of the arc-shaped resonant cavity, the FR1 shows a redshift, and the phenomenon is consistent with Eq. (4). In addition, as previously analyzed, the generation of FR2 is related to the rectangular stub. As the radius increases, the distance between the rectangular stub and the arc-shaped resonant cavity becomes more significant and is not helpful for the arc-shaped resonant cavity to generate a strong resonance. Therefore, the dip of FR2 shows a blueshift. The sensitivity fitting curves of different radii are drawn out based on the experimental data, as shown in Fig. 6(b). Although the Fano resonance becomes more sensitive to the refractive index when the radius increases to 1.2R, the sensitivity curve becomes more nonlinear when the radius is more significant than 1.15R. Therefore, regarding the sensitivity and linearity, the radius is 1.1R, and the sensitivity reaches 1900 nm/RIU. At this time, R_1, R_2, r_1, r_2, and r_3 are 176 nm, 110 nm, 22 nm, 22 nm, and 22 nm, respectively.

The symmetry of the structure also has an important influence on the curve. When the circles inside the arc-shaped resonant cavity are removed partly or entirely, the blueshift of FR1 will occur. However, it is noteworthy that the middle one of the three circles is more relevant to FR1. Compared with when the left or right circle is removed, the dip of FR1 moves to shorter wavelengths when the middle one is removed. This fact accounts for the theory that the middle circle in the arc-shaped circle is helpful for the reinforcement of FR1. This is the subtlety of the structure designed in this study.

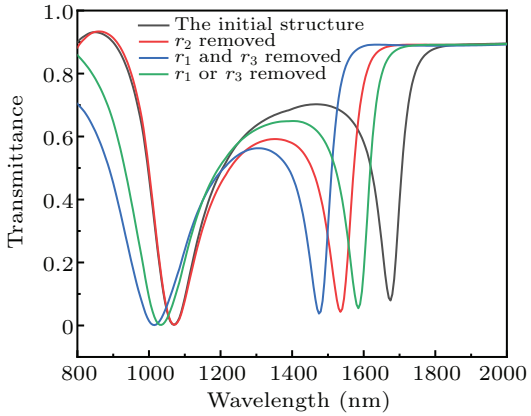


Fig. 7. The transmission spectrum when one or two circles are removed inside the arc-shaped resonance cavity.

4. Conclusion and perspectives

This study presents the MARS structure, which can generate two Fano resonances originating from two different mechanisms. Using the FEM based on the software CMOSOL Multiphysics 5.4, the relationship between the structural parameters and Fano resonance is researched. To understand the formation principles of Fano resonances, this study adds three other structures to conduct comparative experiments. It has been found that the parameter d has a vital influence on the transmittance of FR1, while the height of the rectangular stub mainly exerts its influence on FR2. When R_1, R_2, r_1, r_2, and

r_3 increase, FR1 shows a redshift. In addition, the symmetry of the structure has an important influence on the curve, and the middle circle in the arc-shaped circle is helpful for the reinforcement of FR1. The structure has the advantage of being sensitive to the changes in the refractive index, which is promising for application in various microsensors. The simulation reveals that the sensitivity can reach 1900 nm/RIU and the FOM is 23.75.

Acknowledgements

System numerical simulation was provided by COMSOL, INC.

The work was supported in part by the National Natural Science Foundation of China (Grant Nos. 61875250 and 61975189), the Zhejiang Provincial Natural Science Foundation of China (Grant Nos. LD21F050001 and Y21F040001), the Key Research Project by Department of Water Resources of Zhejiang Province (Grant No. RA2101), the Key Research and Development Project of Zhejiang Province (Grant No. 2021C03019), the Key R&D Projects of Shanxi Province (Grant Nos. 201903D421032 and 01804D131038), and the Scientific Research Foundation of Zhejiang University of Water Resources and Electric Power (Grant No. xky2022032).

References

[1] Barnes W L, Dereux A and Ebbesen T W 2003 *Nature* **424** 824
[2] Jina L, Chen J, Xing L, Tian H, Wang J, Cui J and Rohimah S 2021 *Appl. Opt* **60** 5312
[3] Khani S, Danaie M and Rezaei P 2018 *Optical Engineering* **57** 1
[4] Zhang W 2020 *IEEE J. Quantum Elect.* **56** 1
[5] Gramotnev D K and Bozhevolnyi S I 2010 *Nat. Photon.* **4** 83
[6] Zhang Y, Zhang Y and Dong Z C 2018 *Acta Phys. Sin.* **67** 223301 (in Chinese)
[7] Wang B L 2020 *Chin. Phys. B* **29** 045202
[8] Chen J, Li Z, Li J and Gong Q 2011 *Opt. Express* **19** 9976
[9] Li Y C, Dai X, Jiang J L, Pan J Z, Wei X Y, Lu Y P, Lu S, Tu X C, Sun G Z and Wu P H 2018 *Chin. Phys. B* **27** 060701
[10] Zhou N, Ye C, Polavarapu L and Xu Q H 2015 *Nanoscale* **90** 25
[11] Zhang H, Shen D and Zhang Y 2014 *Laser Phys. Lett.* **11** 115902
[12] Chen J C and Ying Y M 2019 *Results Phys.* **14** 102420
[13] Zhang L, Wang L, Wu Y and Tai R C 2020 *Chin. Opt. Lett.* **18** 9240
[14] Lu H, Liu X M, Mao D and Wang G X 2012 *Opt. Lett.* **37** 3780
[15] Estevez M C, Otte M A, Sepulveda B and Lechuga L M 2014 *Analytica Chimica Acta* **806** 55
[16] Lee B, Na H, Lee I M, Park J, Kim K Y and Lee S Y 2010 *Opt. Express* **18** 598
[17] Zhou W, Li K, Song C, Hao P and Wu Y 2015 *Opt. Express* **23** 413
[18] Butt M A, Khonina S N and Kazanskiy N L 2019 *J. Mod. Opt.* **66** 1038
[19] Tsigaridas G N 2017 *Photonic Sens.* **7** 217
[20] Zhu J and Li N 2020 *Opt. Express* **28** 19978
[21] Zhang Y and Cui M 2019 *J. Elec. Mater.* **48** 1005
[22] Liu X, Li J, Chen J, Rohimah S, Tian H and Wang J 2020 *Appl. Opt* **59** 6424
[23] Zhang Y, Kuang Y and Zhang Z 2019 *Appl. Phys. A.* **125** 13
[24] Qiao L T, Zhang G M, Wang Z S, Fan G P and Yan Y F 2019 *Opt. Commun.* **433** 144